RSC Publishing Faraday Discussions

FD Electrolysis: Degradation Mechanisms In Solid Oxide Cells Operated With Reversing Current

Journal:	*Faraday Discussions*
Manuscript ID:	FD-ART-02-2015-000020.R1
Article Type:	Paper
Date Submitted by the Author:	01-Apr-2015

Complete List of Authors:	Hughes, Gareth; Northwestern, Materials Science and Engineering Railsback, Justin; Northwestern University, Materials Science and Engineering Yakal-Kremski, Kyle; Northwestern University, Materials Science and Engineering; Northwestern, Materials Science and Engineering Butts, Danielle; Northwestern University, Materials Science and Engineering Barnett, Scott; Northwestern University, Materials Science and Engineering

CREATED USING THE RSC REPORT TEMPLATE (VER. 3.1) - SEE WWW.RSC.ORG/ELECTRONICFILES FOR DETAILS
REVIEW Faraday Discussions www.rsc.org/xxxxxx | XXXXXXXX

Degradation of $(La_{0.8}Sr_{0.2})_{0.98}MnO_{3-\delta}$ - $Zr_{0.84}Y_{0.16}O_{2-\gamma}$ Composite Electrodes During Reversing Current Operation

Gareth A. Hughes[a], Justin G. Railsback[a], Kyle J. Yakal-Kremski[a], Danielle M. Butts[a] and Scott A. Barnett[a]*

DOI: 10.1039/b000000x [DO NOT ALTER/DELETE THIS TEXT]

Reversing-current operation of solid oxide cell $(La_{0.8}Sr_{0.2})_{0.98}MnO_{3-\delta}$ - $Zr_{0.84}Y_{0.16}O_{2-\gamma}$ (LSM-YSZ) oxygen electrodes is described. Degradation was characterized by impedance spectroscopy in symmetric cells tested at 800°C in air with a symmetric current cycle with a period of 12 hours. No change in cell resistance could be detected, in 1000 h tests with a sensitivity of ~ 1%/kh, at a current density of 0.5 A/cm^2 corresponding to an overpotential of 0.18 V. At a current density to 0.6 A/cm^2 (0.33 V overpotential) measurable resistance degradation at a rate of 3%/kh was observed, while higher current/overpotential values led to faster degradation. Degradation was observed mainly in the ohmic resistance for current densities of 0.6, 0.8 and 0.9 A/cm^2, with little change in the polarization resistance. Polarization degradation, mainly observed at higher current density, was present as an increase in an impedance response at ~ 30 kHz, apparently associated with the resistance of YSZ grain boundaries within the electrode. Microstructural and chemical analysis showed significant changes in electrode structure after the current cycling, including an increase in LSM particle size and a reduction in the amount of YSZ and LSM at the electrode/electrolyte interface – the latter presumably a precursor to delamination.

1 Introduction

The increasing utilization of intermittent renewable electricity sources is focusing attention on electricity storage technologies that can help match the fluctuating supply with varying demand.[1] The energy storage capacity requirements of this application are quite demanding because of the large grid power levels and the need to store for periods of several hours or more. Pumped hydroelectric is the only storage technology currently being extensively utilized, but geographic requirements will likely limit its more widespread use. A number of different storage methods, including batteries and reversible fuel cells, are also being investigated. An advantage of reversible fuel cells is that the energy is stored using low-cost feedstocks (e.g. water and CO_2), and energy capacity can be increased by increasing storage tank size, while the stack size determines the power capacity. In contrast, in batteries the energy is stored within the electrodes, limiting the extent to which energy capacity can be increased relative to power capacity. Furthermore, the energy is typically stored in relatively expensive electrode materials (*e.g.* oxides such as $LiCoO_2$). However, reversible fuel cells usually have relatively low round-trip efficiency, too low to compete with batteries and other storage technologies.[1a, 1d]

Recently, a higher-efficiency storage method utilizing a reversible solid oxide cell (ReSOC) has been proposed.[2] One key question regarding ReSOCs is the long-term durability. Degradation in ReSOCs is similar to that observed during solid oxide electrolysis, which has been studied in some detail.[3] Delamination of the oxygen electrode (electrolysis anode), typically $(La_{0.8}Sr_{0.2})_{0.98}MnO_{3-\delta}$ - $Zr_{0.84}Y_{0.16}O_{2-\gamma}$ (LSM-YSZ), is the dominant degradation mechanism.[4] Furthermore, reversing current operation does not introduce new degradation mechanisms, and in fact reduces the delamination degradation when compared with DC electrolysis operation.[4-5] It was possible to essentially eliminate degradation at 1.0 A/cm^2 by using a cycle with very short periods of electrolysis separated by fuel cell operation,[5] but such a cycle would not be practical for most storage applications. Current density J (or the electrode overpotential η) has a large impact on the degradation rate, with rapid degradation at 1.5 A/cm^2 (η =0.37 V) but no detectable degradation at 0.5 A/cm^2 (η = 0.18 V).[6] Based on these ReSOC reports, and also prior reports on solid oxide electrolysis cells[3g, 3k], it appears that there is a threshold current density of ~ 0.5 - 1.0 A/cm^2 above which oxygen electrode degradation is fast.

In order to design a ReSOC system and assess its performance and economic viability,[7] it is important to know more accurately the maximum J and η values that are consistent with long-term stable operation. In order to be an economically viable storage method, cell lifetimes should exceed 40,000 h and 2,000 cycles (assuming a ~ 24 h storage cycle). Thus, degradation rates should be < 0.5 %/kh and < 0.0125 %/cycle, assuming that a cell resistance increase of < 25% over the stack life is acceptable. The prior reports discussed above do not provide such detailed information on degradation rates; in particular, there is no information in the critical range from 0.5 to 1.0 A/cm^2.

In the present report, LSM-YSZ composite oxygen electrodes were investigated in order to more accurately determine the effect of J and electrode η on degradation rate in this critical range. (Note that the relative importance of J as opposed to η in causing degradation has not yet been elucidated, so both quantities are included in the present report.) In order to focus on the oxygen electrode, which appears to be the cell component most prone to degradation, symmetrical LSM-YSZ / YSZ / LSM-YSZ cells were tested. This has the advantage of minimizing extraneous degradation effects in full cells that may obfuscate the LSM-YSZ electrode degradation of interest here. Furthermore, symmetric applied current cycles, with equal current densities and times in each direction, were utilized in order to maintain symmetrical electrodes throughout the test despite the tendency for more rapid degradation in electrolysis mode. This enables more straightforward electrochemical impedance analysis.

2 Experimental

LSM-YSZ / YSZ / LSM-YSZ symmetrical cells were fabricated by first die pressing YSZ electrolyte pellets from YSZ powder mixed with 1% PVB binder, and then sintering at 1400 °C for 4 hours. The resulting electrolyte pellets were ~ 0.6 mm thick and 19 mm in diameter. LSM-YSZ electrode functional layers were then screen printed on both sides of the pellets using an ink was produced as follows. A 1:1 mixture (by weight) of $Zr_{0.84}Y_{0.16}O_{2-\gamma}$ (Tosoh) with A-site deficient $(La_{0.8}Sr_{0.2})_{0.98}MnO_{3-\delta}$ (Praxair) was ball milled in ethanol for 24 hr. The solution was

then dried, ground, and passed through a 125 μm mesh sieve. This powder was then added to Heraeus organic vehicle 1:1.18 by weight and fully mixed with a three roll mill. After applying the ink by screen printing, the electrodes were fired at 1175 °C for 1 hour. A current collector layer of LSM ink, made similarly to the LSM-YSZ ink, was then screen printed on top of the LSM-YSZ layer and fired at 1025 °C. The final as-fired thicknesses of the LSM-YSZ functional layer and LSM current collector were both ~ 20 μm thick and had a circular area of 0.5 cm^2. Note that this electrode fabrication procedure is essentially identical to that used in making full cells.

All cells were tested in an open-air furnace at 800 °C. Electrical contacts were made by pressure contacting circular porous LSM current collector pellets, with 0.5 cm^2 area, to the electrodes using a weight of 14 g. LSM was utilized to avoid artifacts that may arise from the transport of noble-metal current collector materials into the electrode active region.[4,8] Current densities between 0.5 A/cm^2 and 1.5 A/cm^2 were applied. Current was applied galvanostatically using a Keithley source meter controlled by a LabView program. The current cycle period was 12 h, with equal times and equal currents in each current direction. The program was paused roughly every 24 hours to run an EIS measurement at open circuit voltage. All cells were tested for ~ 1000 hours.

EIS analysis is simplified in two ways through the use of symmetric cells and current cycles. First, only the oxygen electrode is measured, with no interference from fuel electrode EIS responses as encountered in full cells. Second, by cycling the current with equal periods and amplitudes, each electrode experiences identical conditions, keeping them essentially symmetrical. Thus, electrode impedances are obtained by simply dividing the measured impedances by two. Impedance values are then normalized to the active electrode area, to yield the area specific polarization resistance (R_P) of one electrode and the area specific ohmic resistance (R_Ω) of half the electrolyte.

Although the symmetrical cell test is quite convenient, it is important to consider how well this represents the behaviour of an electrode in a full cell. In a symmetrical cell test, the current/overpotential arises solely from an applied electrical potential, different than a full cell where it arises from a combination of an electrical potential and the chemical potential difference between fuel and oxidant. Nonetheless, a given J should yield the same η for symmetrical and full cells, assuming the same electrode, electrolyte, and oxidant composition. Furthermore, the electrochemical potential gradient across the electrolyte will be the same if both cells have the same current density. Thus, the symmetrical cell tests should provide a very good approximation of the electrode conditions during full cell operation.

Post-test microstructural evaluation was performed on cross sections prepared by first fracturing the cells and then polishing mechanically. Fractured cells were vacuum infiltrated with epoxy (EpoThin, Buehler), cured at 42 °C overnight and the epoxy puck diced with an Accutom 5 saw for SEM mounting. The epoxy helps to give sharp pore contrast and allows for more stable polishing. A cross-sectional surface of the epoxy imbedded cell was then polished to 1 micron with a diamond slurry. The cell was then mounted on an SEM stub for imaging. To prevent charging in SEM, samples were sputter coated with 15 nm of osmium and carbon tape placed close to the cross-sectional surface. Measurements were made using a Hitachi SU8030 Scanning Electron Microscope (SEM) and EDS collected using an Oxford X-max 80 SDD EDS detector. Images and EDS measurements were collected at 20

and 30 keV with a 20 μA probe at a 15 mm working distance in order to gain adequate contrast through the osmium and collect EDS signal from the underlying material.

3 Results

An initial exploratory test was done wherein the current density *J* was increased incrementally in steps of ~150 h, starting at 0.5 A/cm^2 and finishing at 1.5 A/cm^2; this provided an approximate overview of the degradation rate versus *J*, and the results suggest that the degradation rate becomes significant just below ~ 1 A/cm^2. Based on this result, 1000 h life tests were done at current densities of 0.6, 0.8 and 0.9 A/cm^2. Prior data taken with identical cells and an identical test setup, but different current densities of 0.5 and 1.5 A/cm^2, are also shown for comparison.[6] Section 3.1 describes the increasing current test, section 3.2 the constant current test, and section 3.3 the SEM-EDS analysis.

3.1 Incrementally Stepped Cycled Current Density

The incremental test was started at 0.5 A/cm^2 and the current was then increased to 0.7, 0.9, 1.0, 1.1, 1.2, 1.3, 1.4, and 1.5 A/cm^2. The cell was maintained at each *J* for at least 150 hours. The results from selected EIS measurements are shown in Figure 1. The data were fit using the equivalent circuit shown in Figure 1, and an example fit is shown for 1.4 A/cm^2. The fit using two R-Q elements is reasonably good; better fits can be achieved by adding more elements to the model, but the intent here was to quantify the main electrode responses with a reasonably simple model. The two responses have peak frequencies at ~ 100 Hz and 30 kHz. As seen in the Nyquist plot, the ohmic resistance (approximately the high frequency intercept) first decreased during operation at up to ~ 1.2 A/cm^2, before increasing at higher *J*. As seen in the Bode plot, the main change with increasing time and *J* was an increase in the high-frequency response, while the lower frequency response remained approximately constant.

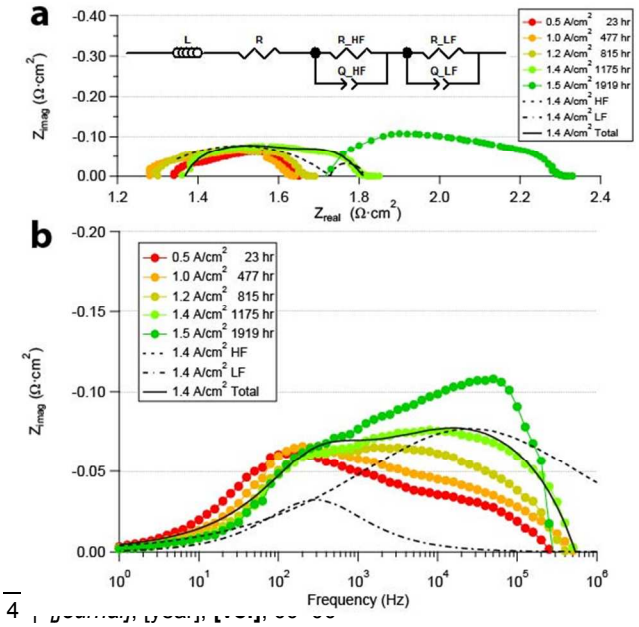

Fig. 1 Nyquist and Bode plots of selected EIS measurements, taken at zero current during brief interruptions in a reversing-current life test in which J was incrementally stepped up to higher values.

Figure 2 shows a plot of measured total, ohmic, and polarization resistances versus time. The values were obtained from the EIS fitting, rather than by observing the real-axis intercepts, in order to minimize errors in determining the intercepts. The same trends that were apparent in Figure 1 are also seen here: the total resistance changes relatively little at the lower J values, but then the resistance increase accelerates with increasing J. The polarization resistance increase begins early on, near 0.5 A/cm^2. However, there was considerable variability of the ohmic and polarization resistance values in Figure 2, a result of errors introduced in the EIS fitting process. This made it difficult to assess their degradation rates given the relatively short constant-current intervals. Thus, the total resistance was used to estimate the onset of significant degradation: the resistance increase appears to begin at > 0.7 A/cm^2, corresponding to η > 0.22 V.

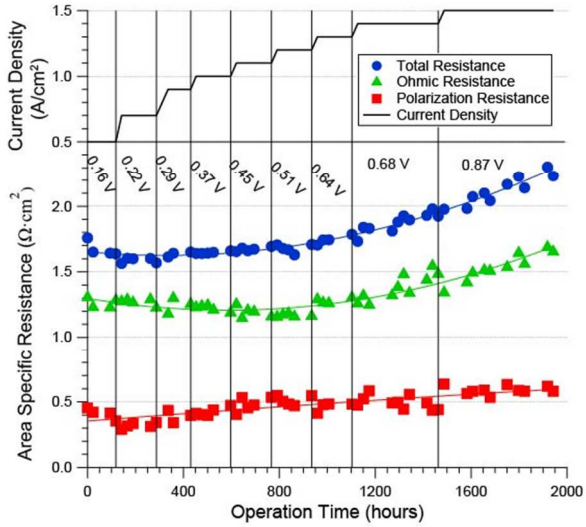

Fig. 2 Total, ohmic, and polarization resistance values versus time during a reversing-current life test in which the current density was incrementally stepped up to higher values. The values are derived from EIS data as shown in Figure 1 from circuit models. The vertical lines separate regions with different constant current densities, with values indicated. Voltage labels are electrode overpotentials at the start of each current step.

3.2 Constant Cycled Current Density

Based on the above results, current densities of 0.6 A/cm^2, 0.8 A/cm^2 and 0.9 A/cm^2 were chosen for three longer-term tests aimed at more accurately assessing the degradation rate. Figure 3 shows the EIS data from the 0.8 and 0.9 A/cm^2 life tests. There were differences between the initial cell responses in the ohmic resistance, due to electrolyte thickness variations. The ohmic resistance clearly increased with

time for both cells. There were also minor differences in the shape of the polarization response, presumably due to cell-to-cell processing variations. On the other hand, after an initial decrease in the lower-frequency peak of the cell tested at 0.8 A/cm^2, the polarization resistance magnitude was almost identical for the two cells. After the initial break-in, the low-frequency response was essentially stable for both current densities. The high frequency response shows a slight increase with time, similar to the changes observed in the cell tested at multiple current densities (Figure 1), but the increases are much less, as expected given the lesser overall degradation observed.

The total, ohmic, and polarization resistance values, obtained from fits to the data in Figure 3, are plotted versus time in Figure 4. Prior data[6] also shown in Figure 4 are from life tests at 0.5 A/cm^2, showing no detectable change in resistance, and 1.5 A/cm^2, showing substantial increases in both ohmic and polarization resistance. In some cases, the cell resistance varied strongly initially, but then stabilized after ~ 70 h. The cell tested at 0.5 A/cm^2 showed a slight steady decrease in R_P that was almost exactly compensated by an increase in R_Ω, such that there was no net change in total resistance. η across a single electrode, calculated from J and polarization resistance, was 0.17 V. For J increased from 0.6 to 0.9A/cm^2 (initial η value from 0.33 to 0.38 V), the rate of decrease of R_P lessened, while the rate of increase of R_Ω increases, resulting in a faster total resistance increase. At J = 1.5 A/cm^2 (initial η = 0.93 V), both R_P and R_Ω increased rapidly with time.

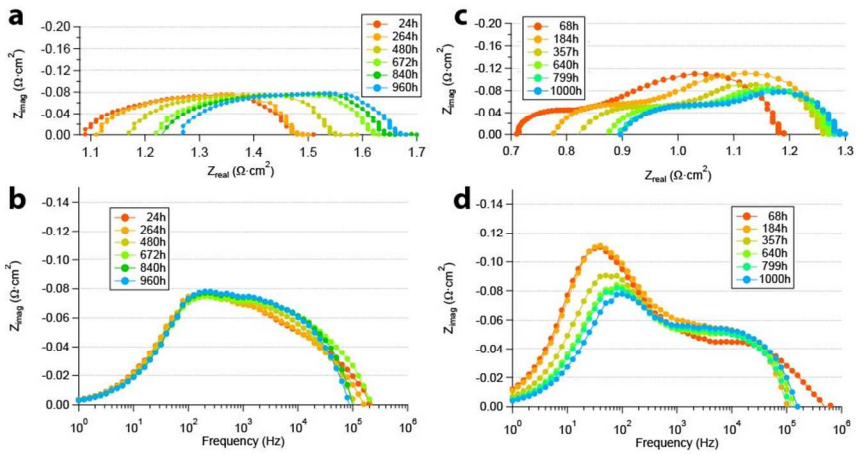

Fig. 3 Nyquist and Bode plots of selected EIS measurements taken at zero current during brief interruptions in reversing-current life tests in which the current density was maintained at (a,b) 0.9 or (c,d) 0.8 A/cm^2.

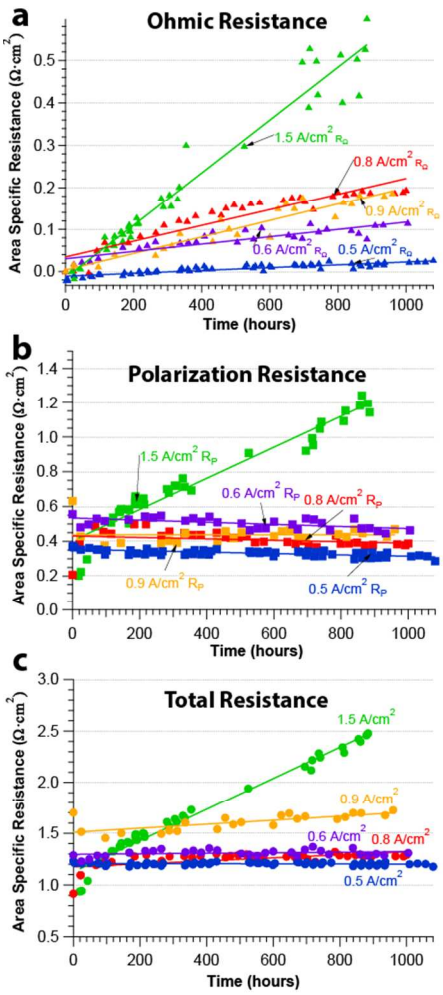

Fig. 4 (a) Ohmic (b) polarization and (c) total resistance versus time during reversing-current life tests at current density values of 0.6, 0.8 and 0.9 A/cm^2. The values are derived from fits to the EIS data shown in Figure 3. Also shown are data from a previous report in which identical cells were tested in the same way in the same test setup at 0.5 A/cm^2 and 1.5 A/cm^2.[6] The initial Ohmic resistance, which varied with electrolyte thickness, has been subtracted in part (a) to allow for easier comparison of the resistance changes.

Fig. 5 plots the measured total resistance degradation rates, obtained from best fits to the cell resistance versus time data in Fig. 4 neglecting any initial break-in

effects, versus η (a) and J (b). The constant-current life tests have relatively small error bars – they appear able to resolve ~ 1 %/kh degradation. However, the life test with incrementally increased current had only ~ 150 h hold times at each J, leading to much larger errors. Despite the relatively large errors in some of the data points, Figure 5 gives a reasonable idea of how the degradation rate increases with current. Furthermore, the constant-current 0.5 A/cm^2 and 0.6 A/cm^2 tests provide a fairly clear indication that measurable degradation starts at a current between these values.

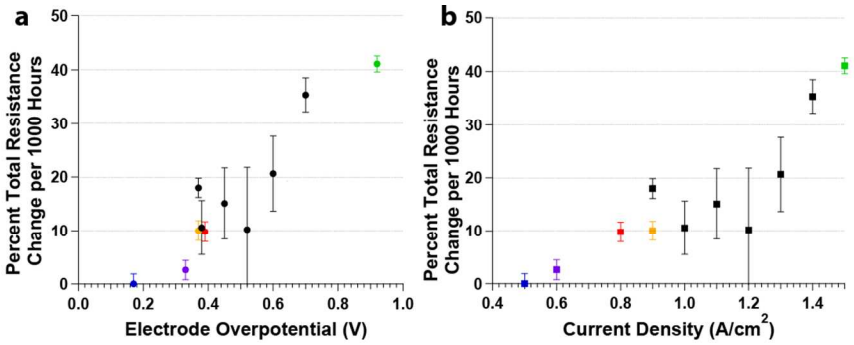

Fig. 5. Degradation rates, derived from the slopes of the total resistance versus time data in Figures 2 and 4, as a function of a) current density and b) overpotential. Colored points correspond to the life tests in figure 4: 0.5 A/cm^2 blue, 0.6A/cm^2 purple, 0.8 A/cm^2 red, 0.9 A/cm^2 yellow, 1.5 A/cm^2 green.

3.3 SEM-EDS Analysis

SEM-EDS analysis was completed on a cell that was annealed with zero current along with the 0.8 and 0.9 A/cm^2 cells. Example images from these are shown in Figure 6. The cell annealed without current shows uniform electrode structure right up to the interface, whereas in the 0.8 A/cm^2 and 0.9 A/cm^2 cases there are microstructural changes near the electrode/electrolyte interface and throughout the active layer. The electrode structure near the electrode-electrolyte interface appears to be depleted of material, containing fewer electrode particles and larger pores. There is significant coarsening of the LSM particles in the active layer for the cells run at 0.8 A/cm^2 and 0.9 A/cm^2, compared to the no-current cell, but the YSZ particles remain un-coarsened. Also, the electrolyte shows pits and pores near the electrode/electrolyte interface, especially in the 0.9 A/cm^2 cell.

The line scans in Figure 7 quantitatively show that La and Mn (i.e., LSM) are depleted near the electrode-electrolyte interface in the 0.8 and 0.9 A/cm^2 samples, in agreement with the images in Figure 6. The La and Mn signals increase with increasing distance from the electrolyte. On the other hand, the main effect of current on the Zr composition profile is a stronger local variation in intensity, presumably related to the presence of enlarged LSM particles.

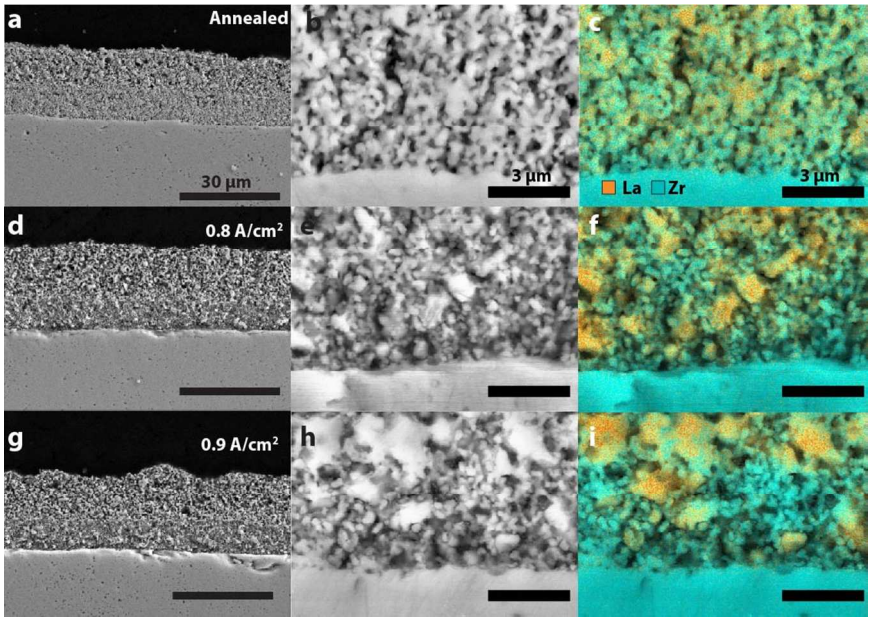

Fig. 6 A summary of: low magnification SEM images (left column), higher magnification SEM images (middle column), and EDS compositional maps (right column) from the electrode/electrolyte regions of cells with no current (top row), 0.8 A/cm^2 (middle row), and 0.9 A/cm^2 (bottom row). The color scheme of the composition maps is shown in the upper right frame.

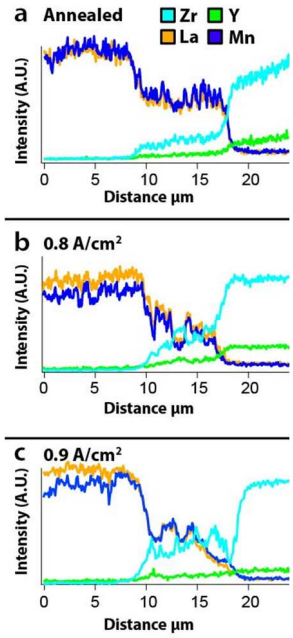

Fig. 7 EDS linescans and corresponding SEM for a) annealed b) 0.8 A/cm^2 and c) 0.9 A/cm^2 cells.

4 Discussion

The present results show that the overall resistance degradation rate increases with increasing current density J (overpotential η), increasing above the present detection limit of 1%/kh for J somewhere between 0.5 and 0.6 A/cm^2 (η = 0.17 to 0.33 V). This result is consistent with SEM observations: substantial changes in the near-interface structure were observed for J = 0.8 and 0.9 A/cm^2 (η = 0.39 and 0.37 V), whereas there was little observable change in structure reported previously (for the same cells and test conditions) at 0.5 A/cm^2.[6] These results are consistent with a recent report[5] where degradation was observed for J = 1.0 A/cm^2 (η = ~0.25 V), unless the fraction of the time in electrolysis mode during the reversing-current cycle was reduced. For J increased above 0.8 A/cm^2 (0.39 V), the rate of degradation increases rapidly to > 10 %/kh, fast enough to severely limit device lifetime and hence the total amount of energy that can be stored/converted. Since it is important to reach degradation rates well below 1%/kh, longer-term measurements at J ~ 0.5 - 0.6 A/cm^2 will be useful in the future to provide greater sensitivity to degradation.

For all J below 1.5 A/cm^2, the degradation appeared to be mainly in the ohmic resistance (Figure 4a), while the polarization resistance showed little change (Figure 4b). In contrast, at 1.5 A/cm^2, both resistance components contributed to the degradation. The ohmic resistance degradation can be understood via the observed formation of voids in the YSZ electrolyte near the electrode/electrolyte interface (see Figure 6 for 0.9 A/cm^2, and Refs[3m, 5]). At higher J (1.5 A/cm^2), where grain boundary pores join and produce extended regions of electrode/electrolyte separation,[6] ohmic resistance presumably also increases by current constriction.

In a previous report on similar LSM-YSZ symmetric cells, the response peaking at ~30 kHz was attributed to the grain boundary transport losses in the electrode YSZ phase.[9] EIS measurements of the present LSM-YSZ cells with varied oxygen partial pressure (not shown) indicated no change in this high-frequency response, providing further evidence that this response arises from an interfacial (e.g., grain boundary transport) resistance. Given that pore formation on YSZ grain boundaries within LSM-YSZ electrodes has been observed after reversing-current operation,[5] it is reasonable to attribute the polarization resistance increase to increasingly resistive YSZ pathways because of degraded electrode grain boundaries. The SEM images in Figures 6 and 7 indicate depletion of YSZ from the electrode near the electrolyte, consistent with this interpretation. That is, formation of voids in the YSZ corresponds to a net local depletion of YSZ.

The SEM-EDS results for 0.8 and 0.9 A/cm^2 suggest that the amount of LSM in the interface region also decreases after cell operation under current. There appears to be a gradual increase in the amount of LSM with increasing distance from the interface, perhaps indicating that material has been transported away from the interface during cell operation. Finally, the LSM particle size within the functional layers has increased after degradation. There does not appear to be a prior report of such changes in the LSM phase in LSM-YSZ functional layers. While there is no obvious explanation, cation transport has been observed in similar perovskite oxygen electrode materials under an oxygen gradient, as was present in the present experiments during cell operation.[10] Given the extensive structural/chemical changes within the electrode functional layer for 0.8 and 0.9 A/cm^2, it is perhaps surprising

that the increases in polarization resistance are not larger. Indeed, SEM-EDS analysis of the electrode/electrolyte interface appears to be a very sensitive means for detecting low levels of degradation, perhaps more so than the EIS measurements.

The apparent removal of material from near the electrode/electrolyte interface presumably represents an early stage of the oxygen-electrode delamination that was reported for LSM-YSZ electrodes after ~ 1000 h at a higher J of 1.5 A/cm^2, both in current switching and electrolysis modes.[6] That is, continuing removal of material ultimately results in a complete interfacial opening or delamination. Such delamination is likely even at the lower J of 0.8 A/cm^2 for sufficiently long-term cell operation.

As discussed previously[6], the degradation during reversing current operation appears to be similar to that seen in dc electrolysis operation, although the periods of fuel cell operation can partially mitigate degradation.[4-5] The degradation presumably occurs during the electrolysis periods of reversible operation. Thus, the present results should be qualitatively similar to dc electrolysis. However, there is relatively little data that is directly comparable. Knibbe et al.[11] showed degradation of full Ni-YSZ/YSZ/LSM-YSZ cells at J = 1 A/cm^2, but the initial η was only 0.19 V. While this is consistent with the J values causing degradation in the present results, no degradation would be expected at this η based on the present data. Note that most of the degradation was observed in the ohmic resistance,[11] similar to the present results. Reports on degradation of LSM electrodes are difficult to compare directly with the present LSM-YSZ results. In one case, delamination was observed after operation at 0.5 A/cm^2,[3l] but the polarization resistance was quite high such that η ~ 3 V, well above the value where degradation is expected. Tests on symmetric LSM electrode cells (on YSZ) showed rapid resistance increases and delamination after 100 h at ~ 2.0 A/cm^2 and η ~ 0.76 V.[3i]

Although there is no definitive experimental evidence showing whether J or η controls oxygen electrode degradation, models of the degradation mechanism suggest that η is the controlling parameter. Models are generally based on the large electrochemical oxygen potential developed near the electrode/electrolyte interface.[3i, 3l, 3m] This high effective oxygen pressure can drive the observed nucleation of oxygen bubbles in the region near the electrode-electrolyte interface.[3m] In one case, a critical η required to nucleate oxygen bubbles in YSZ was predicted to be 0.28 V.[12] The present results, where the η value sufficient to cause degradation was between 0.18 V and 0.33 V, are consistent with this predicted value. Other models are based on $La_2Zr_2O_7$ formation[3i] and LSM lattice contraction[3l] due to the high oxygen potential, but these do not predict potential values where degradation is expected.

5 Conclusions

The present results represent an attempt to determine the J and η values below which LSM-YSZ electrode degradation becomes negligible during reversing current operation. The following conclusions can be made:

1. EIS tests over ~ 1000 h on symmetrical cells appear able to detect a degradation rate of 1%/kh.
2. SEM observations appear to be quite sensitive to the early stages of degradation, as seen by a decrease in the apparent amount of LSM and YSZ at the interface, and an increase in the size of LSM particles in the functional layer.

3. The present results show that degradation caused by reversing-current operation can be reduced below ~ 1%/kh, the present detection limit, by operating at a current density between 0.5 A/cm^2 and 0.6 A/cm^2 with an oxygen electrode overpotential between 0.18 V and 0.33.
4. At higher current densities and overpotentials, the degradation rate increases rapidly, leading to device lifetimes that would be too short for practical application;
5. EIS measurements show a unique signature associated with the degradation – an increase in a high-frequency (~10^4 Hz) response – which appears to be associated with YSZ grain boundary transport losses. This could be a sign of oxygen bubble formation on grain boundaries.

6 Acknowledgements

The authors gratefully acknowledge financial support from the Global Climate and Energy Project at Stanford University Project under award 51922. The development of the cell test setup and the image interpretation were also supported by the Department of Energy Basic Energy Science program (Grant # DE-FG02-05ER46255). SEM analysis made use of the EPIC facility (NUANCE Center-Northwestern University), which has received support from the MRSEC program (NSF DMR-1121262) at the Materials Research Center, and the Nanoscale Science and Engineering Center (EEC-0118025/003), both programs of the National Science Foundation; the State of Illinois; and Northwestern University.

7 References

[a] *Department of Materials Science and Engineering, Northwestern University, 2220 Campus Dr., Evanston, IL 60208, USA Email: s-barnett@northwestern.edu Phone: +18474912447*

1(a) Z. G. Yang, J. L. Zhang, M. C. W. Kintner-Meyer, X. C. Lu, D. W. Choi, J. P. Lemmon and J. Liu, *Chem Rev*, 2011, **111**, 3577; (b) D. o. E. ARPA-E, Seattle, 2009; (c) R. M. Dell and D. A. J. Rand, *Journal of Power Sources*, 2001, **100**, 2; (d) B. Dunn, H. Kamath and J. M. Tarascon, *Science*, 2011, **334**, 928; (e) J. Liu, J. G. Zhang, Z. G. Yang, J. P. Lemmon, C. Imhoff, G. L. Graff, L. Y. Li, J. Z. Hu, C. M. Wang, J. Xiao, G. Xia, V. V. Viswanathan, S. Baskaran, V. Sprenkle, X. L. Li, Y. Y. Shao and B. Schwenzer, *Adv Funct Mater*, 2013, **23**, 929.

2(a) D. M. Bierschenk, J. R. Wilson and S. A. Barnett, *Energy Environ. Sci.*, 2011, **4**, 944; (b) P. Kazempoor and R. J. Braun, *International Journal of Hydrogen Energy*, 2014, **39**, 5955.

3(a) J. Malzbender, P. Batfalsky, R. Vaßen, V. Shemet and F. Tietz, *Journal of Power Sources*, 2012, **201**, 196; (b) Y. L. Liu, K. Thydén, M. Chen and A. Hagen, *Solid State Ionics*, 2012, **206**, 97; (c) H. Yokokawa, H. Y. Tu, B. Iwanschitz and A. Mai, *Journal of Power Sources*, 2008, **182**, 400; (d) M. J. Jørgensen, P. Holtappels and C. C. Appel, *Journal of Applied Electrochemistry*, 2000, **30**, 411; (e) J. R. Wilson, J. S. Cronin and S. A. Barnett, *Scr. Mater.*, 2011, **65**, 67; (f) Z. Zhan, W. Kobsiriphat, J. R. Wilson, M. Pillai, I. Kim and S. A. Barnett, *Energy & Fuels*, 2009, **23**, 3089; (g) A. Hauch, S. H. Jensen, S. Ramousse and M. Mogensen, *J. Electrochem. Soc.*, 2006, **153**, A1741; (h) A. Hauch, S. D. Ebbesen, S. H. Jensen and M. Mogensen, *J. Electrochem. Soc.*, 2008, **155**, B1184; (i) M. Keane, M. K. Mahapatra, A. Verma and P. Singh, *International Journal of Hydrogen Energy*, 2012, **37**, 16776; (j) J. R. Mawdsley, J. D. Carter, A. J. Kropf, B. Yildiz and V. A. Maroni, *International Journal of Hydrogen Energy*, 2009, **34**, 4198; (k) C. Graves, S. D.

Ebbesen and M. Mogensen, *Solid State Ionics*, 2011, **192**, 398; (l) K. Chen and S. P. Jiang, *International Journal of Hydrogen Energy*, 2011, **36**, 10541; (m) A. V. Virkar, *International Journal of Hydrogen Energy*, 2010, **35**, 9527.

4 G. A. Hughes, K. Yakal-Kremski, A. V. Call and S. A. Barnett, *J. Electrochem. Soc.*, 2012, **159**, F858.

5 C. Graves, *Solid Oxide Fuel Cells 13 (Sofc-Xiii)*, 2013, **57**, 3127.

6 G. A. Hughes, K. Yakal-Kremski and S. A. Barnett, *Physical chemistry chemical physics : PCCP*, 2013, **15**, 17257.

7(a) P. Kazempoor, C. H. Wendel and R. J. Braun, *Ecs Transactions*, 2014, **58**, 45; (b) S. D. Ebbesen, S. H. Jensen, A. Hauch and M. B. Mogensen, *Chem Rev*, 2014, **114**, 10697; (c) U. S. D. o. Energy, 2013.

8 S. P. Simner, M. D. Anderson, L. R. Pederson and J. W. Stevenson, *J. Electrochem. Soc.*, 2005, **152**, A1851.

9 J. S. Cronin, K. Muangnapoh, Z. Patterson, K. J. Yakal-Kremski, V. P. Dravid and S. A. Barnett, *J. Electrochem. Soc.*, 2012, **159**, B385.

10 M. Oh, A. Unemoto, K. Amezawa and T. Kawada, *Solid Oxide Fuel Cells 12 (Sofc Xii)*, 2011, **35**, 2249.

11 R. Knibbe, M. L. Traulsen, A. Hauch, S. D. Ebbesen and M. Mogensen, *J. Electrochem. Soc.*, 2010, **157**, B1209.

12 O. Comets and P. W. Voorhees, *Electrochemical Synthesis of Fuels 1*, 2012, **41**, 123.